Use of FEM models to study fatigue of overhead contact wires

J.-P. Massat[1], E. Balmes[2 3], J.-P. Bianchi[3]

[1] SNCF, Engineering department, St Denis, France
[2] Arts et Métiers ParisTech, PIMM, Paris, France
[3] SDTools, Paris, France

Abstract

Fatigue cracks can induce fracture of the catenary Contact Wire (CW) and thus huge costs for the operator. Nowadays the wear criterion to replace the CW leads to lifespan over than 50 years, and the catenary can see a very high number of cycles so that fatigue life must be taken into account.

A full process to compute the multiaxial transient stress field in the CW has been developed. A fatigue criticality indicator to assess the risk of crack initiation was introduced. This elaborate indicator is used to validate a simplified fatigue indicator based on the uniaxial Euler-Bernoulli beam stresses that are much faster to compute. This indicator is then used to assess parameters influencing the risk of fatigue in the case of junction claws.

Keywords: Catenary, contact wire, fatigue, wear, modelling.

1 Introduction

With a high speed network more than 35 years old and more than 800 trains operated every day, SNCF has a solid feedback in catenary maintenance and design of a High-Speed infrastructure patrimony. SNCF developed an economic maintenance strategy based on equilibrium between maintenance and regeneration expenses. The infrastructure design strategy also considers the whole system by a continuous optimization of the interaction between infrastructure and rolling stock.

With targeted maintenance actions and improvement of components, the catenary lifetime has been extended to more than 50 years. However, this extension may lead to new failure modes that have to be taken into account in the maintenance strategy in order to avoid unpredictable failures that have a huge impact on traffic disruption, client discomfort (delays, speed slowdowns) and associated costs.

1

This paper is focused on renewal of contact wires which is currently based on wear rate. On high speed lines, the wear rate is almost negligible and the contact wire lifetime is estimated over 60 years. However, the overhead contact line of the first high speed line (1980) was already renewed because the commercial speed was increased from 270km/h to 300km/h and also because some fatigue failures occurred due to inappropriate component maintenance for high speed conditions.

A theoretical and practical study was carried out to analyse parameters that significantly influence the fatigue phenomenon. A numerical study associated with laboratory testing was handled to determine leading physical phenomena. Indeed, this failure mode results of interaction of all aspects of contact wire life: design (mechanical tension, material properties), building (methodology of unrolling contact wire), system (quality of dynamic interaction with the pantograph), maintenance (contact wire wear rate), etc.

Fatigue studies need to compute stresses in the Contact Wire (CW). OSCAR [1] is the tools used by SNCF to study the dynamic interaction between pantograph and catenary. The catenary is meshed using beam elements, and stress could be evaluated using the Euler-Bernoulli formalism. But the occurrences of crack initiation were typically reported in transition areas (claws, …), where the validity of a beam model can be doubted. For this objective, a process for evaluations of 3D stresses compatible with the simulation of a full catenary section has been developed (Bianchi [2]) and is detailed in section 2.1. This process is an extension of the standard OSCAR computations with the ability to include a 3D wire segment.
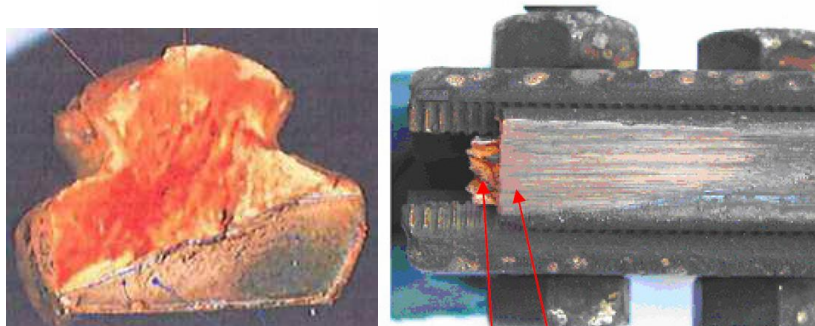

Figure 1 : Sample reported ruptures

Section 2.2 illustrates that the CW sees mostly bending deformation so that the axial component of stress is the main contributor in fatigue analyzes. Section 2.3 details the level of error found when only using beam stresses rather than the real volume stresses.

In section 3, effects influencing criticality are analyzed in detail. Claw position within a span, interactions between claws and droppers and wear are thus shown to have significant impact on stresses viewed in the wire. Such studies can be used to orient maintenance guidelines.

2   Stresses and fatigue analysis

Fatigue analyses need to know the stress cycle at given point of the CW. OSCAR models are based on beam elements so that only uniaxial stress can be computed. A full volume model strategy to compute the six components of the transient stresses has first been developed and is detailed in section 2.1. Section 2.2 introduces the criticality indicator used to evaluate fatigue and the typical stress cycles of a CW point when a pantograph is passing. Section 2.3 compares the uniaxial stress computed through a beam model of CW with the axial component of the full stress field, and goes back to the criticality indicator.

2.1   Methodology to compute 3D stresses

The general method, detailed in this section and summarized in Figure 2, aims at computing stresses at any point of a CW. Two models are defined from OSCAR standard model of catenary which combines beams, bar and mass elements. The first mixed model combines the OSCAR model and volume mesh of an area of interest (study area). It is used to compute 3D static stresses and an expansion basis. The second model is a standard beam model refined or adapted to have a number of coincident nodes with the mixed model. This adapted beam model is used to compute the dynamic displacements that will be expanded to estimate the dynamic part of the 3D transient stresses in the mixed model.
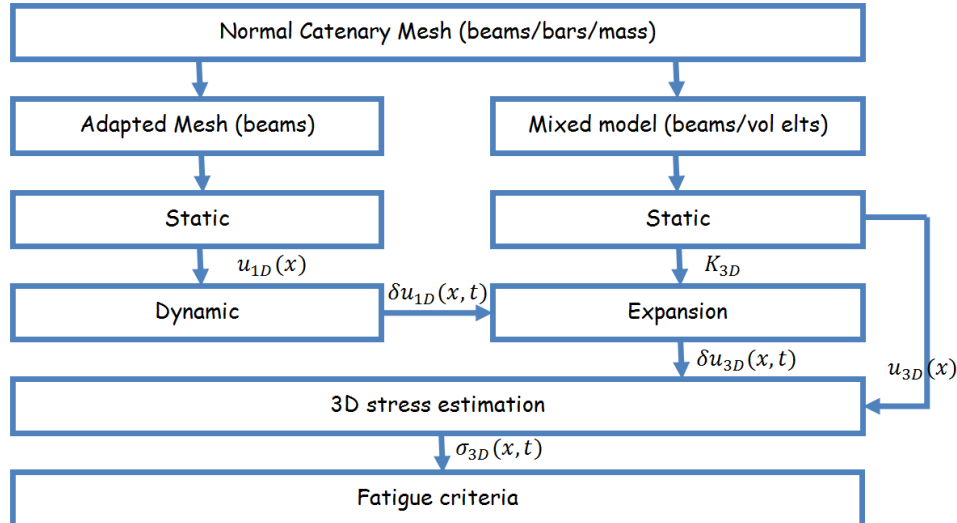

Figure 2: General process for stress computations.

The first step of the considered strategy is to generate a standard OSCAR mesh (Figure 3a) that is composed of pre-stressed beams and mass elements. Then an area of interest, where fatigue study will be performed, is meshed in detail using volume elements: a CW segment of a few meters and all claws connected to this segment: junction claw, dropper claw… The volume mesh is inserted in the beam mesh replacing beams, connecting the CW volume mesh extremities to adjacent beams

3

through rigid link rings (Figure 3c), and the dropper claws to the dropper through RBE3 ring (Figure 3d). This results in the mixed model of Figure 3b.

<table>
<tr><td>(a)</td><td>(b)</td><td>(c)</td><td>(d)</td></tr>
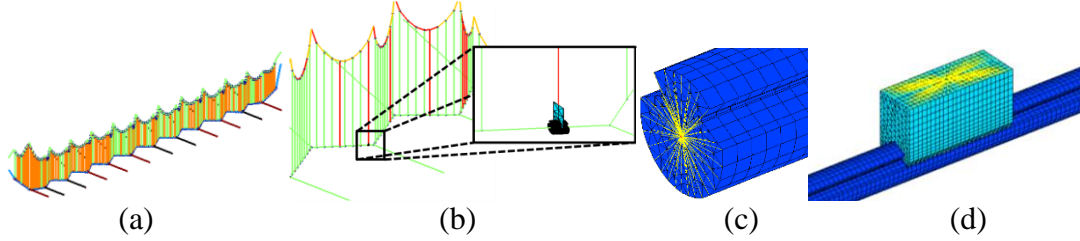</table>

Figure 3: Parts of the mesh. (a) OSCAR original mesh. (b) Mixed model. (c) Rigid link ring at 3D part extremity. (d) Dropper claw connection.

The 3D study area is generated by automated meshing of wire and claw sections followed by an irregular extrusion. The resulting elements are pentahedra. Element size is varying in CW section around 1 mm, and the extrusion step is typically 2 mm. The length of the 3D study area varies from 1.5 to 2 meters leading to model sizes in the 500 000 to 700 000 DOF range.

The adapted model is generated from the initial OSCAR model, and the mesh of the study area. The adaptation consists mainly in refining the beams in the study area to have coincident nodes on the neutral fiber of the CW. This adaptation is key to obtain a correct expansion for the dynamic displacements: the adapted model must give an accurate beam/bar/mass representation of the mixed model.

The second step is a non-linear static resolution of the mixed model taking in account gravity, pre-stress in beam elements, and full geometric non-linearity in the volumes. At each iteration step, one considers residuals in the "1D" (beam/bar/mass elements) and "3D" parts (volume mesh of the study area).

In the beam wires (1D part) the tension is adjusted leading to a change in the tangent stiffness in beam elements. This change in tangent stiffness is the only effect of geometric non-linearity. Unilateral stiffness in the droppers is also accounted for. The 1D residual is thus given by

$$\{R_{1D}(q^n)\} = [K_{1D}(q^n)]\{q^n\} - \{F_{gravity} + F_{Tension}\} - \{F_{NL}(q^n)\} \tag{1}$$

In the volumes, the full Green-Lagrange strain

$$\{e\} = \frac{1}{2}\left(FF^T - I\right) = \frac{1}{2}((I + \nabla u)(I + \nabla u)^T - I) \tag{2}$$

is computed and is related to the Piola-Kirchoff stress $\{S\}$ by an elastic law

$$\{S\} = \lambda Tr(e)I + 2\mu e \tag{3}$$

and leads to the 3D residual

$$\{R_{3D}(q^n)\} = \int_\Omega F_{gravity}.dv - \int_{\Omega_0} S(q^n):\delta e \tag{4}$$

The nonlinear solution then seeks to minimize residuals through iterations on q^n. Linear constraints associated with the beam/volume connections are handled by elimination. One starts from a zero state and considers displacement increments

4

$$\{\delta q\} = \{q^{n+1}\} - \{q^n\} = [T][J(q^n)]^{-1}\{R(q^n)\} \tag{5}$$

that verify the constraints. It is noted that the current computation does consider constraints in the nominal geometry, when updating these constraints to account for the large transformation might be needed.

A typical computation time for 3D static and expansion matrix is 2 hours.

A full dynamic computation on the mixed model would represent a too high computation time. Besides geometry transition between beam and volume meshes would be a very complex task (contact strategy, wave reflections problems...) in the dynamic problem.

The proposed solution, is thus to expand the response of the adapted model. The resolution of the adapted model transient is a standard OSCAR run takes less than 10 min for a full section. The simulation uses a Newmark implicit scheme with Newton iterations, and accounts for beam pretension, dropper unilaterality, and pantograph moving contact.

Static and dynamic solutions of the adapted mesh lead to transient solutions

$$u_{1D}(x,t) = \left(u_{stat,1D}(x) + \delta u_{1D}(x,t)\right) \tag{6}$$

decomposed in a static part $u_{stat,1D}(x)$ and a dynamic part $\delta u_{1D}(x,t)$. It is then assumed that the full 3D response can be decomposed in a non-linear static part and a linearized dynamic solution

$$u_{3D}(x,t) = u_{stat,3D}(x) + [T](\delta u_{1D}(x,t)) \tag{7}$$

where recovery of the 3D displacement from beam motion to full 3D response is obtained using the static reduction/condensation basis [T] (Guyan [3]).

Since the rotations are not present in volumes, a strategy to couple beam rotation DOFs and volumes is needed. One thus considers six independent loads, shown in Figure 4, on a ring of nodes around the neutral axis. From these loads, one builds a series of static deformation shapes of the mixed model so that observation of translations and rotations on the adapted model mesh part correspond to unit translations and rotations, thus leading to the reduction basis.
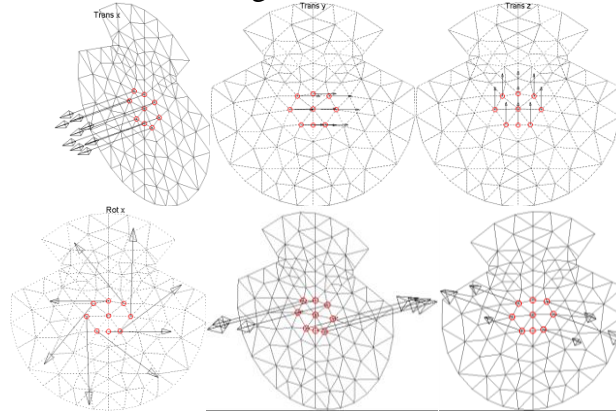

Figure 4: Unit loads corresponding to 6 interface DOFs of Guyan condensation.
Top: translations, bottom: rotations.

5

Stresses are linearly related to displacements. It is thus possible to build an observation equation for stresses at specific positions and use the expansion (7) to obtain

$$\sigma_{3D}(x,t) = [c]\left(u_{3D,stat}(x) + \delta u_{3D}(x,t)\right) = \sigma_{3D,stat} + [cT]\delta u_{1D}(x,t) \qquad (8)$$

where the static stress $\sigma_{3D,stat}$ and the stress observation matrix $[cT]$ can be precomputed so that the application of (8) has a very low cost. Rich parametric studies on train configuration can thus be performed with a single time consuming 3D run.

2.2 Fatigue criticality and σ_{xx} component

The full volume process has been used to compute the multi-axial stresses in the CW. With the full 3D stress field, a multi-slope Dang Van criterion can be computed at any point of the contact wire to assess the risk of crack initiation. The unlimited endurance domain has been precisely identified for the common copper alloy used for CW. The criticality of a given cycle due to a train passage is quantified by a scalar called criticality ("Cd" in the figures). This coefficient is directly linked to an expected lifespan before crack initiation, in each point of the contact wire.
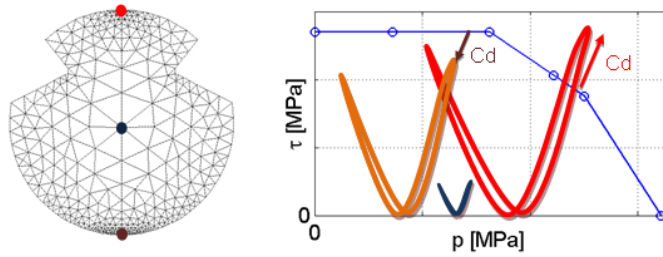

Figure 5: Dang Van criterion at 3 points of a CW section (red on top, blue at center, orange at bottom).

With the Dang Van theory, the six stress components are necessary. However, other studies demonstrated that the criticality is mainly driven by σ_{xx} component. For instance, Figure 6 shows a configuration with a junction claw followed by a dropper. The added bending stiffness leads to a major drop of axial stress under the claws. The left image shows that the cycle is mainly composed by bending due to the vertical load from the pantograph. The amplitudes of the other five stress components are low compared to σ_{xx} (maximum of amplitude of σ_{xx} : ~230 MPa, σ_{yy} : ~8 MPa, σ_{zz} : ~4 MPa, σ_{yz} : ~0.3 MPa, σ_{zx} : ~1.7 MPa, σ_{xy} : ~2.5 MPa).
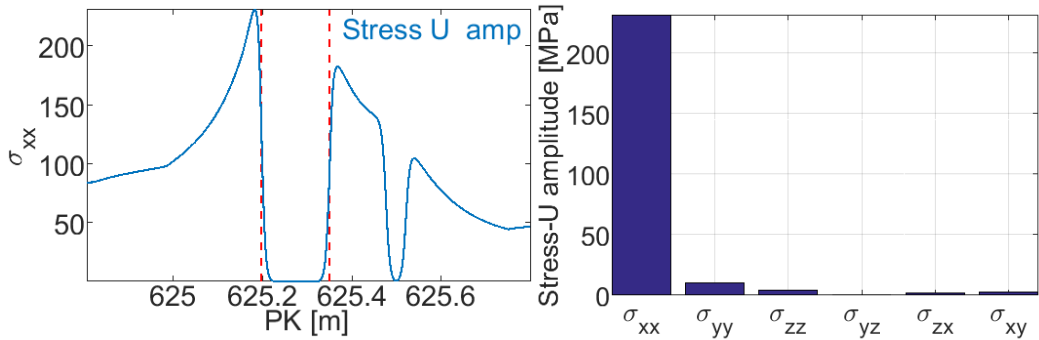
Figure 6: Left: Amplitude component of σ_{xx} volume stress at the top of CW. Junction claw extremities in red dashed lines. Dropper claw @625.5m. Right: maximum of amplitude of each stress components.

Figure 7 shows the time evolution of the stress components at a given point located before the junction claw, at the top of the CW. The main stress is σ_{xx}, and other components are very low: we can consider that the deformation of the CW when the train is passing is almost pure bending.
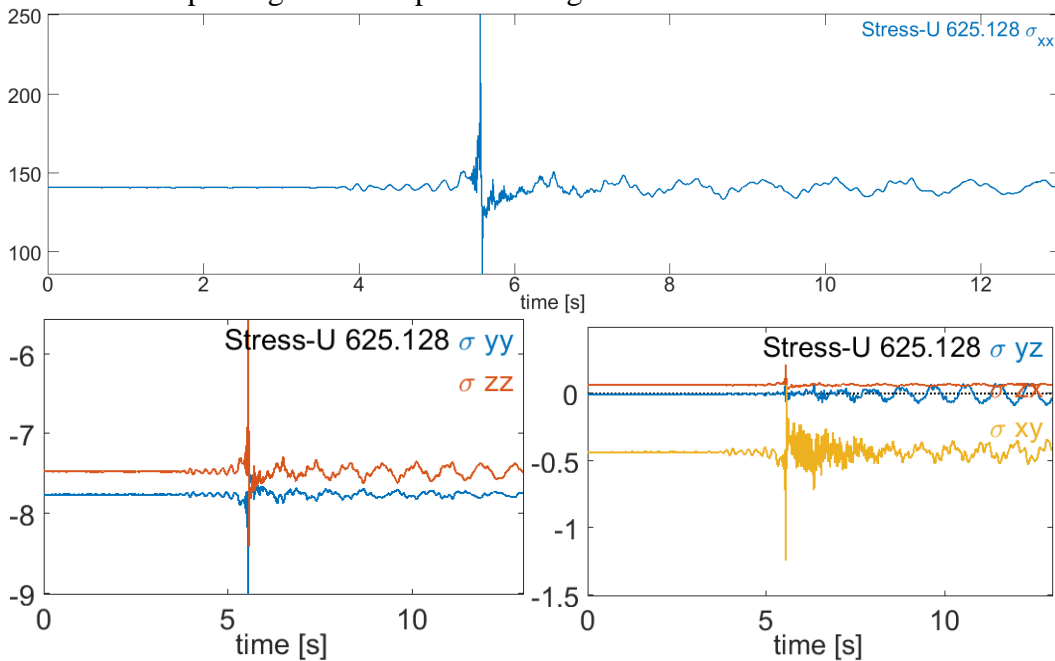

Figure 7: Stress components at the top of the CW at a given point before the junction claw. Up: σ_{xx}. Dow left: σ_{yy} and σ_{zz}. Down right: σ_{yz}, σ_{zx} and σ_{xy}.

Figure 8 compares the corresponding Dang Van path computed with the full 6 stress component cycle in blue line to the Dang Van path computed with only the σ_{xx} component in red line (other component considered constant at 0 MPa). The V shape is expected for a bending cycle. The criticality of a given cycle is mainly driven by the mean and the amplitude of the stress field. The amplitude of the red cycle is the same as the blue because stress amplitudes other than σ_{xx} are very low, but translated because of static value of other components that sligthly differ from 0.
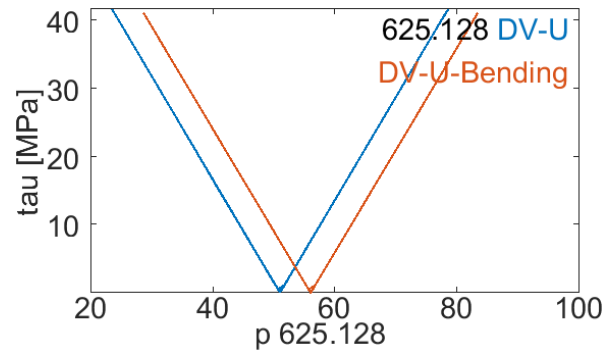
7

Figure 8: Dang Van diagram at the top of the CW at a given point before the junction claw. Blue: real Dang Van path. Red: Dang Van path with only axial component of the stress.

Considering that the deformation of the CW is mostly bending, the Dang Van path cycle should be mostly related to the axial stress component. Figure 9 top shows the 3D criticality obtained on about 100 m of high speed catenary, on the top and bottom line of the CW. Outside singularities such as junction claws, the criticality remains under 0, that is to say that there is no risk of crack initiation.

The lower part of Figure 9 shows the criticality (Cd) versus the amplitude of the σ_{xx} component of multi-axial stresses, for all points on the top of the CW (blue) and the bottom of CW (green). A more critical case with a junction claw is added on the same graphs. The correlation between Cd and σ_{xx} amplitude is very high and the relation is linear.

One can thus conclude that the multiaxial aspect of the Dang Van criterion does not have a major influence here and the amplitude of the σ_{xx} component can be considered as a good fatigue indicator, linearly correlated to the elaborate fatigue criterion (Cd) that has been developped.
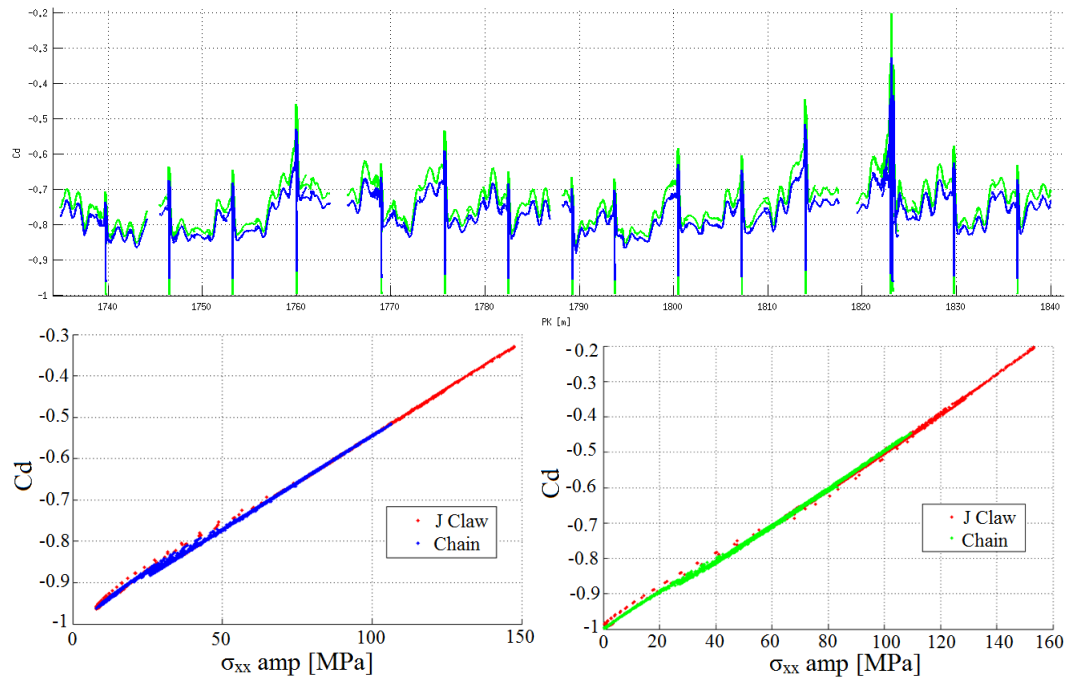
8

Figure 9 : Criticality (Cd). Up: Against position (blue: bottom of CW; green: top of the CW). Down: Cd against the amplitude of σ_{xx} stress component. Left: at the bottom of the CW. Right: at the top of CW. Red: the junction claw case.

2.3 Beam and volume stresses

In this section, the axial component of the volume stresses is compared with uniaxial stress computed in the initial Euler-Bernoulli beam model of the catenary.

As illustrated in Figure 10, the amplitude of σ_{xx} computed in the full volume process only differs from the beam stress in the vicinity of the claws. There beam stresses tend to over-estimate the real axial stress. The relative difference between maximum of σ_{xx} computed in the beam model and in the volume model is 16.5 % at the bottom of the CW and 19 % at the top of the CW. The position of the maximum is also slightly different: with beam stress it is located at the first extremity of the junction claw and for the axial component of volume stress it is a few centimeter before.
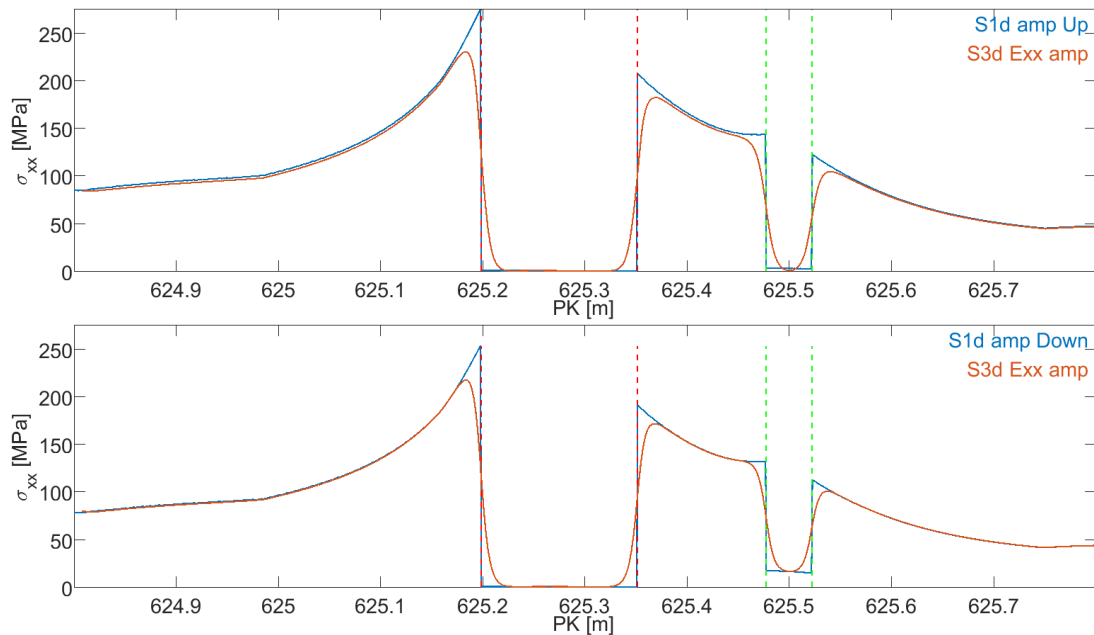
9

Figure 10: Amplitude of σ_{xx}. Blue: uniaxial stress from beam model. Red: σ_{xx} component of the multiaxial stresses computed in the full volume process. Up: at the top of the CW. Down: at the bottom of the CW. Junction claw extremities in red dashed lines, dropper claw in green dashed lines.

Going back to the criticality indicator, illustrates the variation of the amplitude of uniaxial stresses and the criticality on a short area where there is a dropper claw and a junction claw. The σ_{xx} decrease around the claw is brutal whereas Cd decrease is more progressive. That leads to points that strongly differ from the linear relation between Cd and σ_{xx} amplitude but these points are not critical.
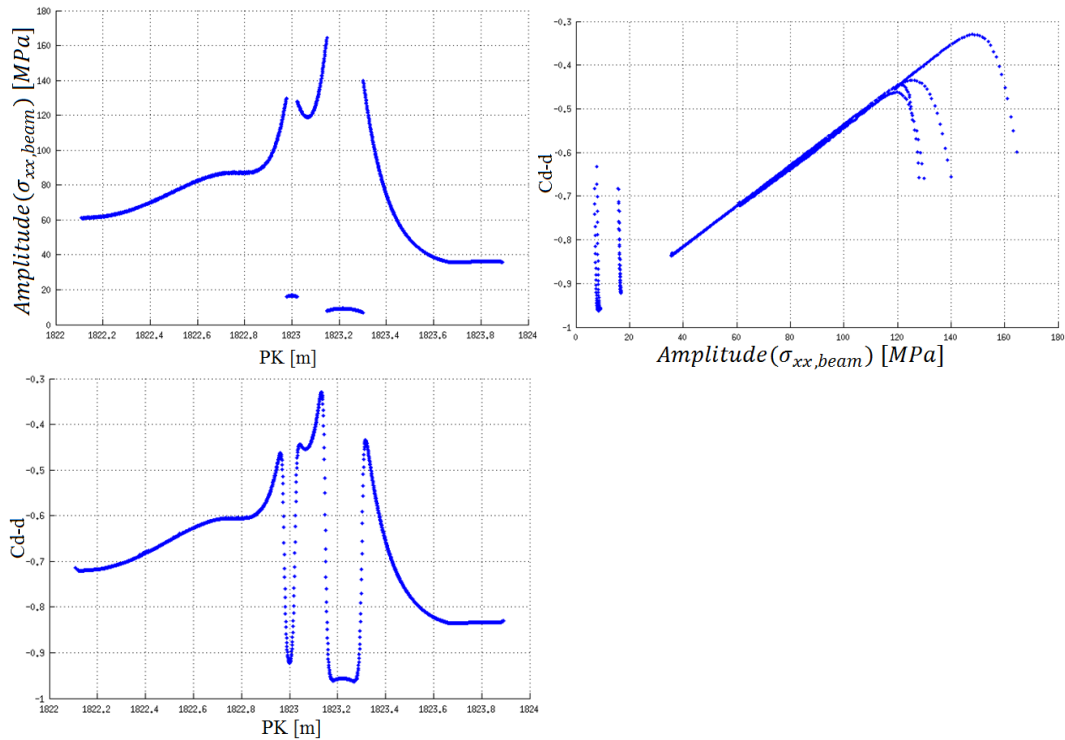
10

Figure 11: Left/Up: beam uniaxial stress amplitude. Left/Down: Cd. Right: Cd against uniaxial stress amplitude.

Considering a set of computations on two spans without any junction claw, the maximum of uniaxial stress amplitude on each of the 3D study areas (1.2-2.5m) is almost linearly linked to the maximum of criticality on the same area, as illustrated in Figure 12. However two close but different lines can be observed. The different line is clearly due to study areas around dropper claws where the uniaxial stress amplitude has a peak that is not found in the Cd curve.
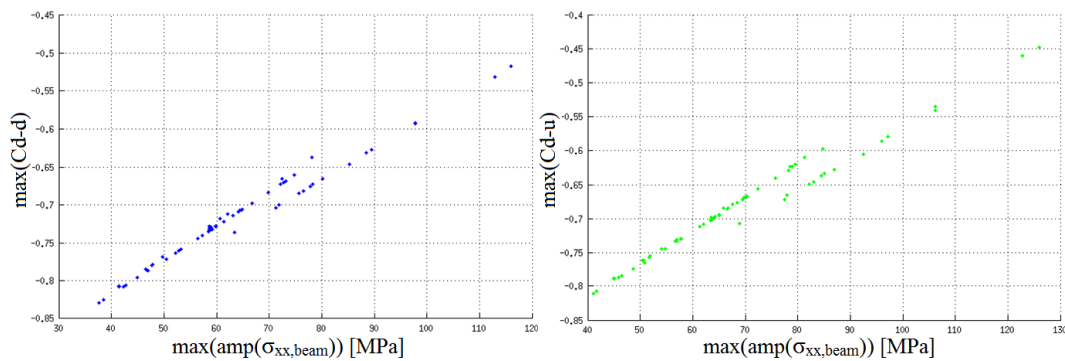

Figure 12: Maximum (on the study areas) of Cd against maximum (on the same area) of uniaxial stress amplitude. Left (and blue): at the bottom of the CW. Right (and green): at the top of the CW.

To conclude this section, uniaxial beam stress is actually a very good approximation of the σ_{xx} component of the multi-axial stresses. On a given study area, computing beam stress during a train passage takes around 10 min whereas the

11

full volume process takes around 2h. We can then have faster an estimation of the maximum fatigue criticality in the area of a singularity, and perform richer parametric studies. Finally, the amplitude of uniaxial beam stress is a good indicator of fatigue criticality, which despite its non absolute nature, can be used to sort the criticality of different configurations.

3 Parameters influencing fatigue criticality

3.1 Influence of position

The first influent parameter considered here is the position a junction claw with the span. A high speed catenary is considered with a pantograph of a simple unit train passing at 300 km/h. The position of the junction claw is varied in a span near the middle of the catenary section. Figure 13 illustrates that the maximum amplitude of stress is globally more important for a junction claw located at the span extremities than near its middle. And a peak is typically visible before droppers.

A first major peak is found for a claw located 22.5 cm before the first dropper of the span. This case will be detailed in sections 3.2 and 3.3. The figure also shows an even higher peak just before the last dropper in the span but this case was identified later and will not be analyzed in detail in this paper.
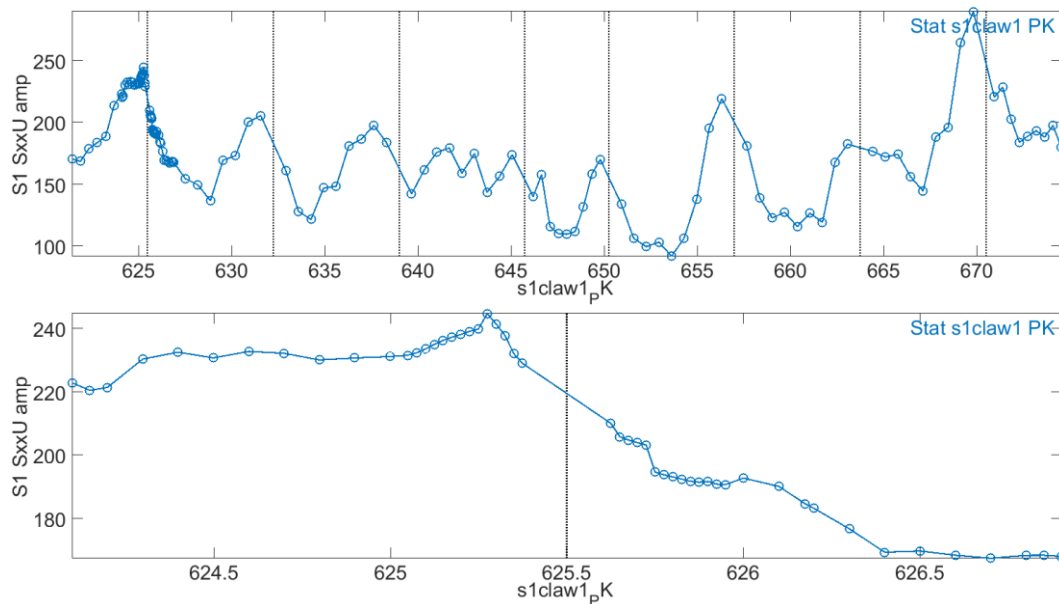

Figure 13: Maximum of amplitude of upper line uniaxial beam stresses against the position of the junction claw. Top: on the full span. Down: zoom around the first dropper.

Figure 14 illustrates the amplitude of uniaxial beam stresses on the lower line of CW. It has the same shape than at the top of the CW but with somewhat lower levels. The fatigue risk is lower accounting only the mechanical analysis, but there are a lot of other phenomena neglected in simulations that can be preponderant

there: electric arcs due to pantograph/CW contact losses, shocks or friction with pantograph, heating, wear...
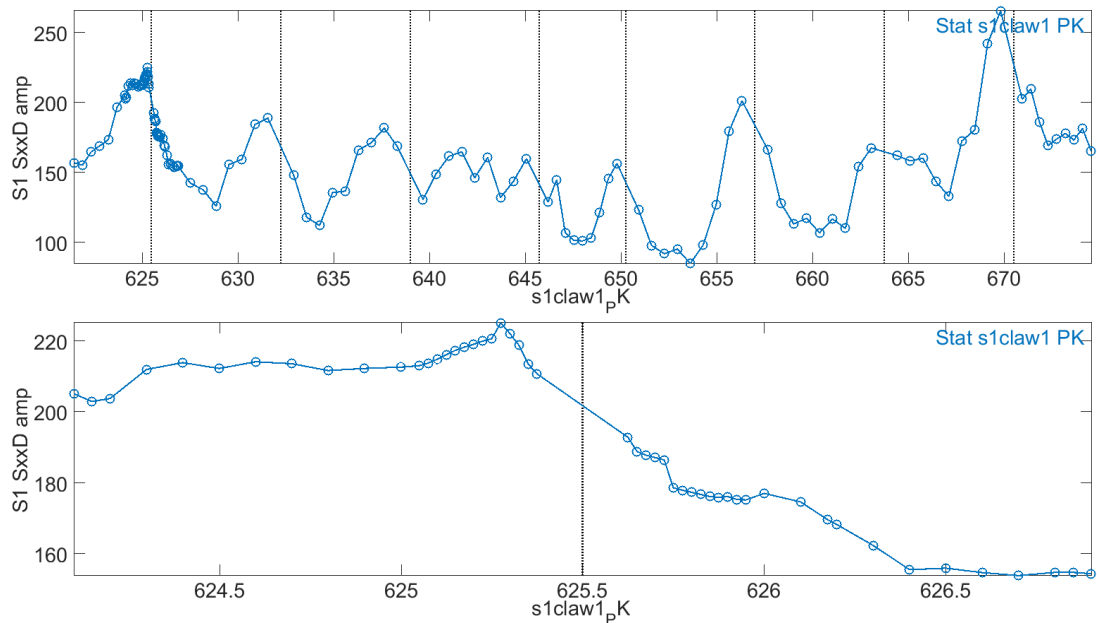

Figure 14: Maximum of amplitude of lower line uniaxial beam stresses against the position of the junction claw. Top: on the full span. Down: zoom around the first dropper.

3.2 Interactions between claw and dropper

As Figure 13 illustrated a stress range peak for a claw located 22.5 cm before the first dropper, this case is analyzed in more detail here. As visible in Figure 15, the spacing between the junction and dropper claws is then about 12.6 cm.
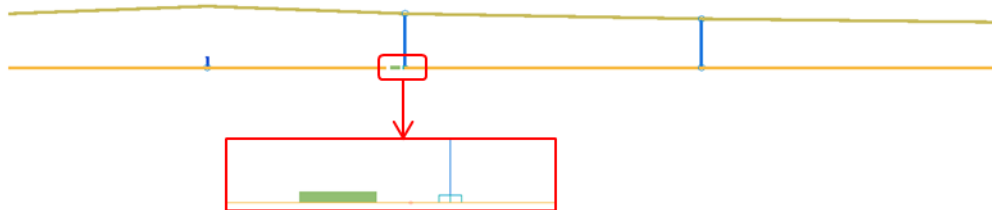

Figure 15: Mesh of the considered case. In green junction claw, in light blue dropper claw, in orange CW, in blue the droppers.

Beam stress color maps in space/time domain around the junction claw are displayed Figure 16. Under the junction and the dropper claws, the stress is always low, because the claws are clamped to the CW and thus a part of the static tension of the CW passes in the claw. Besides the CW/claw part is very stiff (section is more important than elsewhere) so that the level of bending in the wire strongly decreases under the claws.

When the pantograph arrives near the junction claw, its inertia prevents wire motion and its section prevents bending, so that wire bending is localized before the

13

claw. There is an increase of the stress before the claw on the top of the CW due to its upward bending and the corresponding decrease on the bottom line. A similar behavior is found at the claw exit.
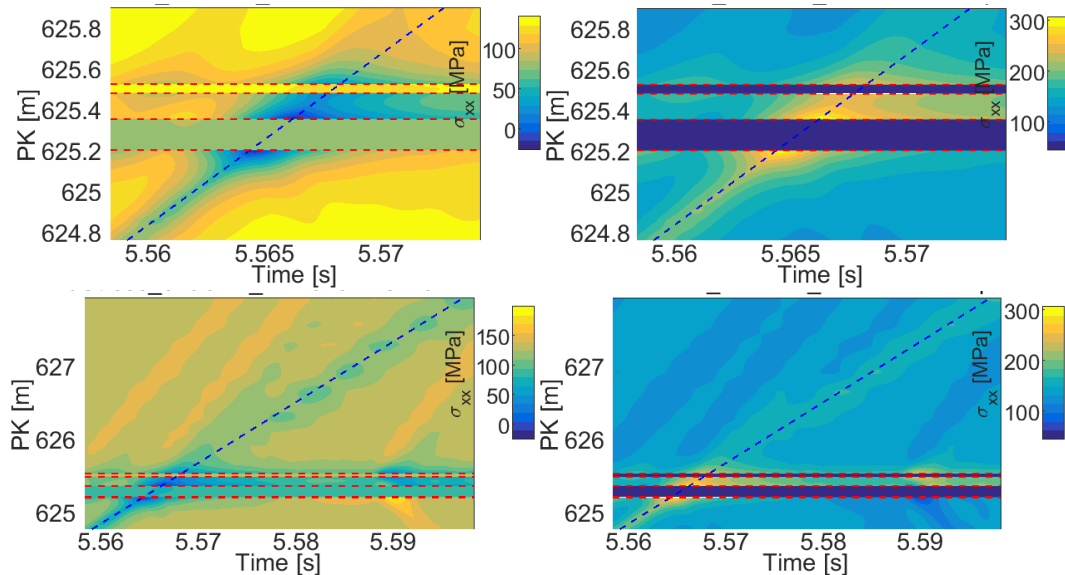

Figure 16: Axial stress on lower line (left) and upper line (right) of CW. Space/time color map. Red dashed lines: extremities of claws. Blue dashed line: position of the train. Top: zoom around the claws.

The specific position of junction claw chosen here is interesting because a second stress peak occurs about 0.02 s after train passage. Figure 17 displays the time evolution of stresses at 3 points of the CW: far from junction claw, just before the junction claw, and just before the dropper claw, on the upper and lower line of CW. Those stress curves are compared to the tension of the dropper in the vicinity of the junction claw.

Far away from the claw and other singularities (blue curves), stresses show a peak at the pantograph passage, and very low fluctuation around ~130 MPa that corresponds to the static stress induced by the CW tension. This corresponds to the usual effect of wire bending due to pantograph passage.

Just before the junction claw, there is an important peak on the upper line (corresponding to a decrease-peak on the lower line). 0.02s later the same point sees a strong decrease of stress, which will augment the stress amplitude and thus the criticality of this configuration.

14

Figure 17: Up (resp. Down): Uniaxial beam stresses at upper (resp. lower) line of CW (blue: far away from junction claw, red: just before junction claw, orange: just after dropper claw). Middle: Tension in dropper. Junction claw @625.275m.

The important stress decrease is due to an interaction with the dropper. When the pantograph is arriving, the dropper is compressed so that tension decreases to 0 N (compression force in the dropper is compensated in OSCAR). After train passage, the wire is moving down, and the dropper gets brutally tensed. The load applied to the CW results in a significant drop of stress in the junction claw entry which increases stress amplitude and thus criticality. Near the dropper claw entry, two stress peaks are found: positive on top of the CW and negative at the bottom. But these do not augment the stress range and are thus not expected to have a major influence.

3.3 Influence of wear

Wear of contact wire is a phenomenon that affects the catenary dynamics, and the interaction with the pantograph. Even though global wear ratio is very low on high speed lines, the CW can be locally worn at higher level near the singularities, in particular near the junction claws, as illustrated Figure 18. Understanding the

potential effects of wear, in particular at specific points such as junction claws, thus seems important for fatigue studies.
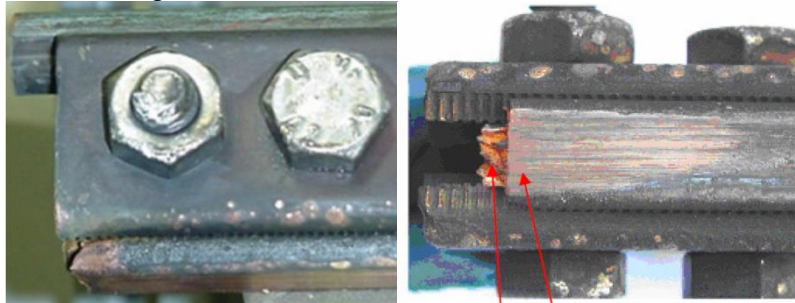

Figure 18: CW worn under two junction claws where ruptures have been reported.

A non-uniform wear has then been introduced in the model, with the following assumptions:

- Variable beam sections are defined for each beam element but the neutral axis is assumed to be straight.
- Variation of the position of the contact line is accounted using geometric irregularity. The contact is handled by penalization, and irregularity is added to the distance from pantograph head to the neutral axis of the CW. This irregularity is interpolated linearly.

The pantograph model is updated to take into account the Contact Strip (CS). Indeed the CS has flexibility whose effect can be visible in the response.

A first computation is performed on a catenary with no wear. The raw contact force is illustrated Figure 19. The contact force near the junction claw shows a peak but clearly bigger peaks are seen elsewhere in the span. However there is clear contact loss (contact force equals zero) after the junction claw.
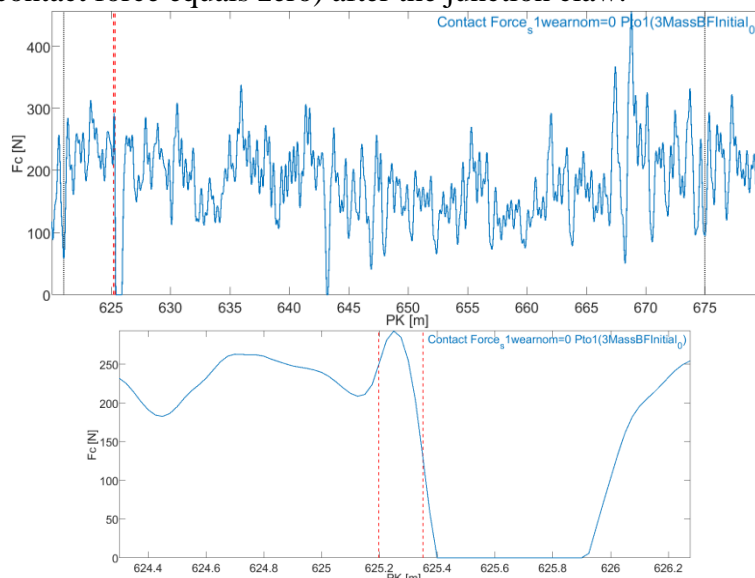

Figure 19: Contact force (raw), GPU model of pantograph with CS (First free bending mode at 200 Hz), no wear. Top: on the full span. Down: zoom around junction claw.

From this first computation, a wear profile is defined by scaling the raw contact force between 0 and a maximum wear value. 21 simulations are performed for a maximum value of wear from 0 % to 20 % of the wire section worn.

Figure 20 shows the geometric irregularity applied to model wear near the junction claw, for all the computed wear levels (from 0 % to 20 %, the wear of 20 % is reached later in the span corresponding to the maximum of contact force in the unworn case as said below). For the highest wear level considered here, the geometric irregularity is 2.5 mm over a 15 cm length ending with no wear in the contact loss area.
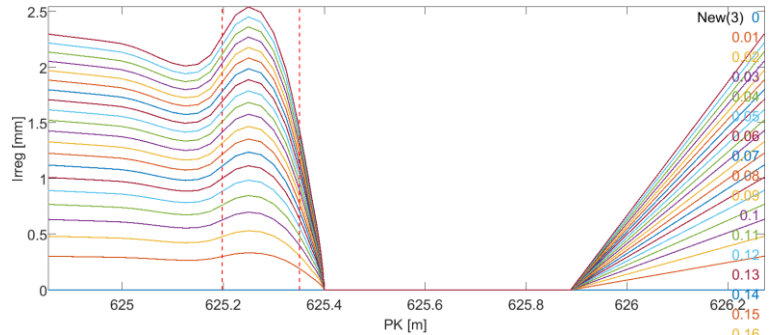

Figure 20: Profiles of wear irregularity (mm) against position (m) for maximum wear. Red dashed lines: Junction claw extremities.

For different levels of wear, Figure 21 shows the contact forces and the maximum and amplitudes of stresses. For sufficient wear, the contact force starts to show a very visible peak after the junction claw, which would certainly be detected in inline measurements. In term of stresses, the wear profile induces a notable stress increase with more impact between the dropper and junction claws than before the junction claw. The amplitude and thus the fatigue criticality follow the same trend.
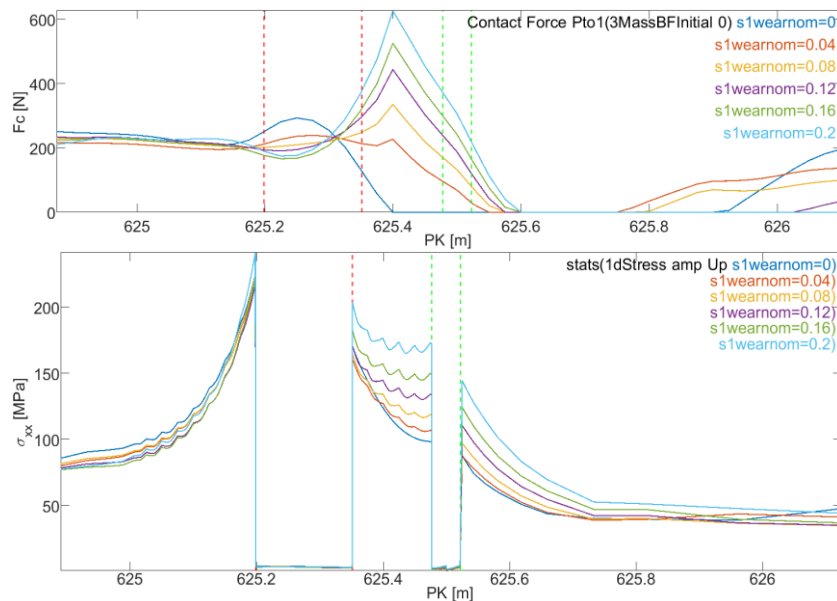

Figure 21 : Up: raw contact force. Down: amplitude of axial stress. Red dashed lines: Junction claw extremities. Green dashed lines: Dropper claw extremities.

To complete the analysis, Figure 22 shows the maximum of stress on the wire as a function of time and the location of this maximum. The small steps at the beginning correspond to the pantograph motion away from the claw. Then for a long period the stress is the highest at the claw entrance. A little after passage of the pantograph at the claw mid-point the maximum stress goes the claw exit and stays there with a small excursion near the dropper claw.
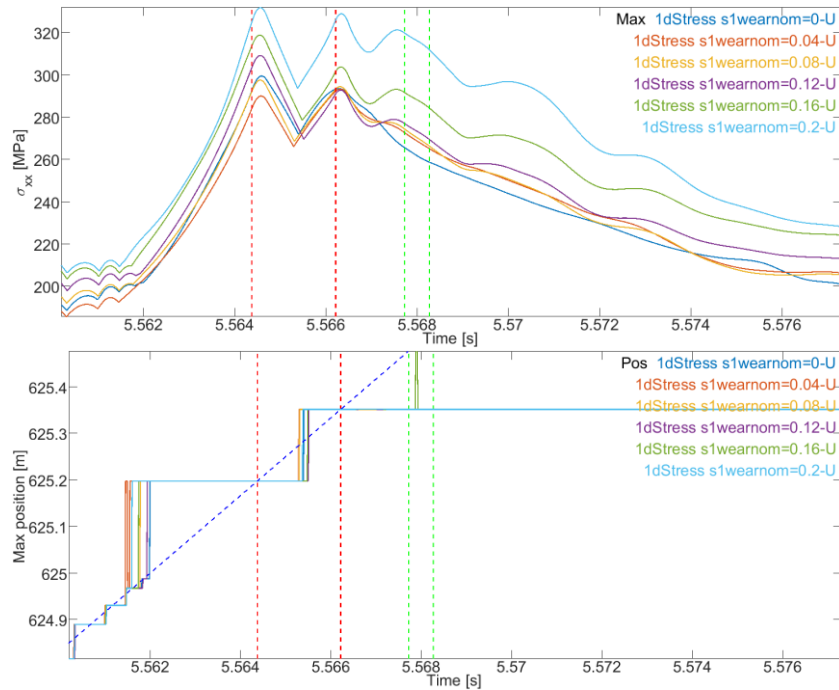

Figure 22 : Up: space maximum of axial stresses against time. Down: at which position this maximum occurs. Red dashed lines: Junction claw extremities, green dropper claw. Blue dashed line: pantograph passage.

Figure 23 top shows the evolution of the σ_{xx} amplitude with the wear level. The amplitude oscillates with the wear level, but it is the highest for the more important wear level considered (20 %). The point where maximum of σ_{xx} amplitude is reached is the first extremity of the junction claw. Figure 23 bottom illustrates the time evolution of the axial stress at the entry of the claw for different level of wear. The evolution of maximum and minimum of stress at this point is not clear. For the wear level of 20 %, the amplitude is maximum and the peak due to the train passage is the higher but the decrease-peak due to the dropper that is going back to its tensed state is the lower.
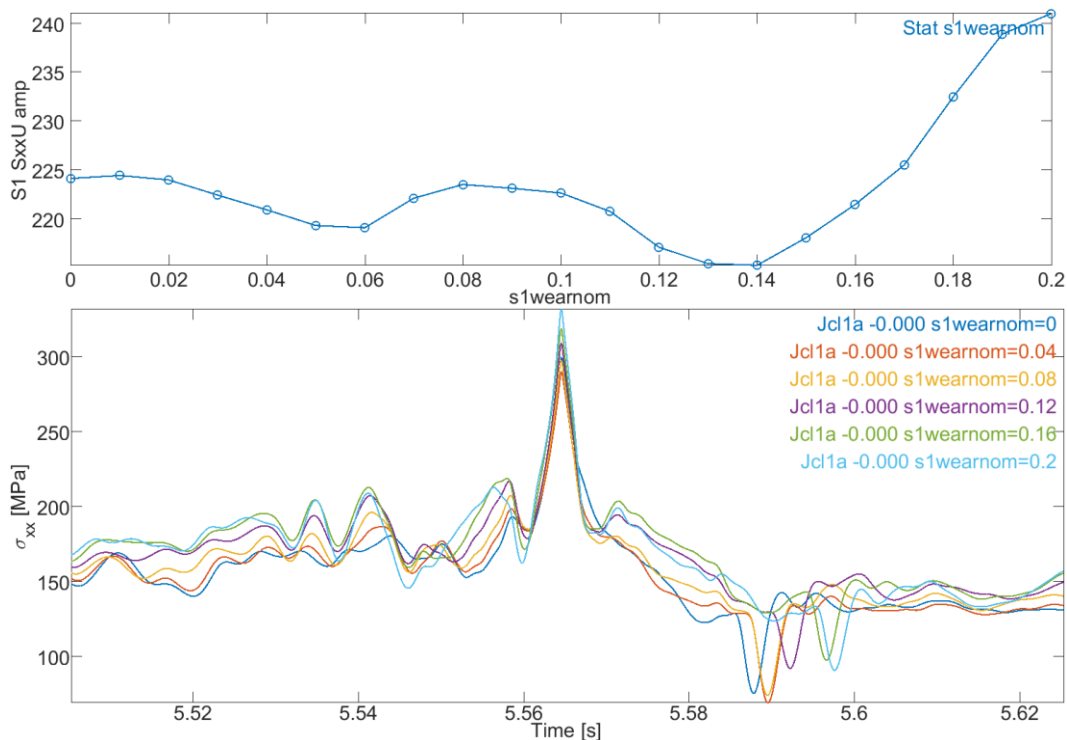
Figure 23 σ_{xx} stress at the top of the CW. Up: maximum of amplitude. Down: time evolution of the stress at the entry extremity of the junction claw.

4   Conclusion

The full fatigue process that has been detailed in this paper has been used to validate an approximated indicator of fatigue which is the beam model uniaxial σ_{xx} stress amplitude. This approximation can be done because the deformation of the CW when a train is passing is mostly bending. This indicator is of course less precise than the Cd fatigue criticality computed through the full volume process: it tends to over-estimate fatigue criticality, the localization of the critical point is not perfect and the absolute value has no real sense (we can't predict a time to live before crack initiation unlike for Cd indicator). This is due to the Euler-Bernoulli theory which is known to be false near singularities, such as the junction claw here. However this indicator is a good estimator of fatigue criticality, and can be used to hierarchize the criticality of different cases. Computation time is much lower and enables to perform very rich parametric studies.

Main result of the study with beam models is to target the junction claw positions which are more critical in terms of fatigue. These are located near and before dropper, with most critical droppers being the first and the last droppers. The case of the first dropper has been studied in detail and shows that the junction claw vicinity with dropper claw induces an interaction that is increasing the fatigue risk: the dropper that is going back to its tensed state after the train passage tends to brutally stop the wire descending motion, that generates downward bending before the junction claw and thus a low level peak in the stress that increases its amplitude and thus the fatigue risk. The local wear effect near the junction claw (that is due to

contact force important variations in this area) has also a strong impact on the fatigue criticality. A clear perspective is cycling simulation to account for wear evolution (indeed, when the CW is worn, contact force is not the same, and so the new wear has not the same shape). More realistic simulations based on real wear profile near the junction claw would also be of great interest.

References

[1] Jean Pierre Massat, Etienne Balmes, Jean Philippe Bianchi, Guido Van Kalsbeek, "OSCAR statement of methods", Vehicle System Dynamics, Vol 53 Issue 3. DOI: 10.1080/00423114.2015.1005016

[2] J.P. Bianchi & E. Balmes & M.L. Nguyen-Tajan, "Dynamic stress prediction in catenary wire for fatigue analysis", IAVSD 2015.

[3] R.J. Guyan, "Reduction of Mass and Stiffness Matrices", AIAA Journal volume 3.